Electronic Supplementary Information

High-Performance Aqueous Zn-MnO_2 Batteries Enabled by the Coupling Engineering of K^+ Pre-intercalation and Oxygen Defects

Kun Han,[a] Fuqiang An,[a] Fengsheng Yan,[a] Hailong Chen,[b,*] Qi Wan,[c] Yongchang Liu,[a] Ping Li,[a,*] Xuanhui Qu[a]

[a] Beijing Advanced Innovation Center for Materials Genome Engineering, Institute for Advanced Materials and Technology, University of Science and Technology Beijing, Beijing 100083, PR China;

[b] The Woodruff School of Mechanical Engineering, Georgia Institute of Technology, Atlanta, Georgia 30332, United States.

[c] School of Materials Science and Engineering, Southwest University of Science and Technology, Mianyang 621010, PR China.

*Corresponding authors.

E-mail addresses: ustbliping@126.com, hailong.chen@me.gatech.edu

a

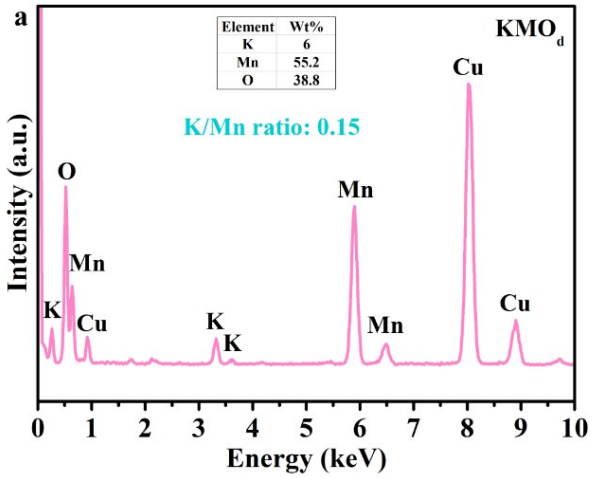

b

ICP-OES Results	
Samples	**K/Mn ratio**
KMO_d (KMO)	**0.15**
α-MnO_2	**0.02**

Fig. S1 (a) Energy dispersive X-ray (EDX) spectrum of KMO_d. (b) Inductively coupled plasma optical emission spectrometer (ICP-OES) results of KMO_d, KMO, and α-MnO_2.

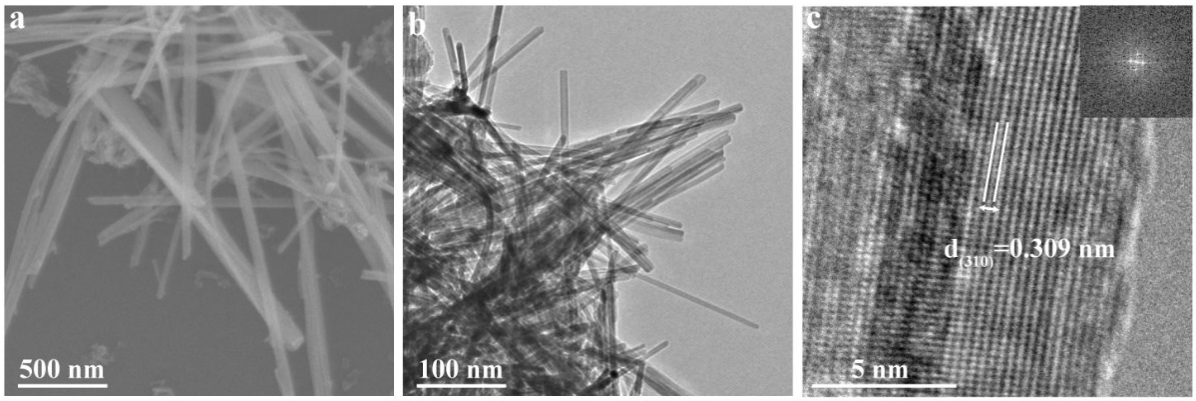

Fig. S2 (a) FESEM image, (b) TEM image, and (c) high-resolution TEM image of α-MnO_2. The inset shows the corresponding FFT pattern.

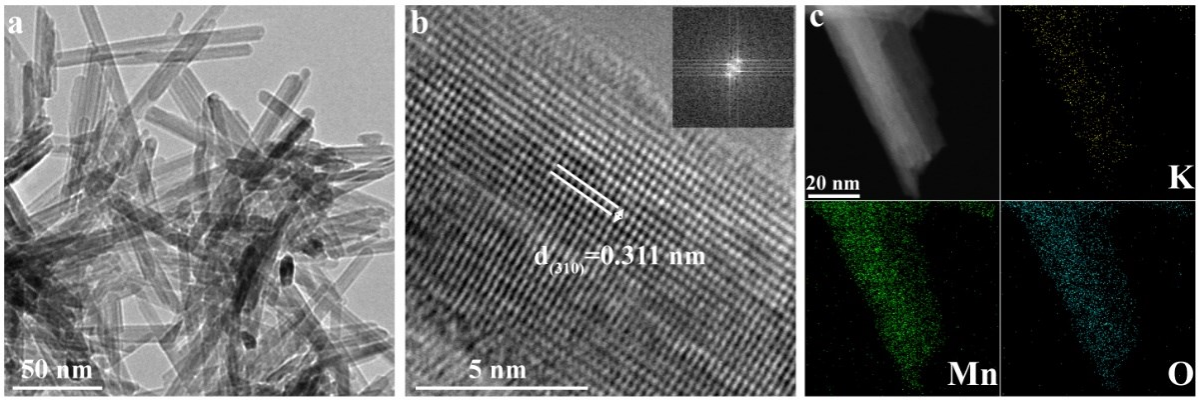

Fig. S3 (a) TEM image, (b) high-resolution TEM image, and (c) HAADF-STEM image and corresponding elemental mappings (K, Mn, O) of KMO. The inset shows the corresponding FFT pattern.

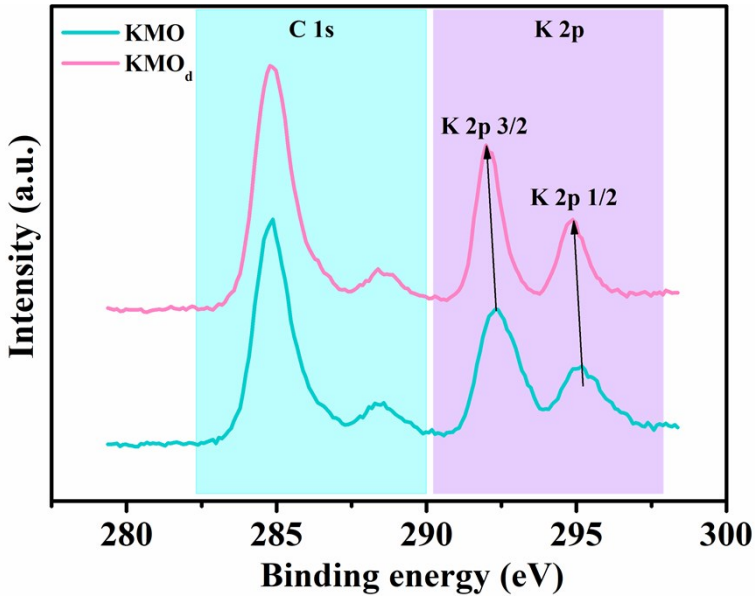

Fig. S4 K 2p and C 1s high-resolution XPS spectra of KMO_d and KMO.

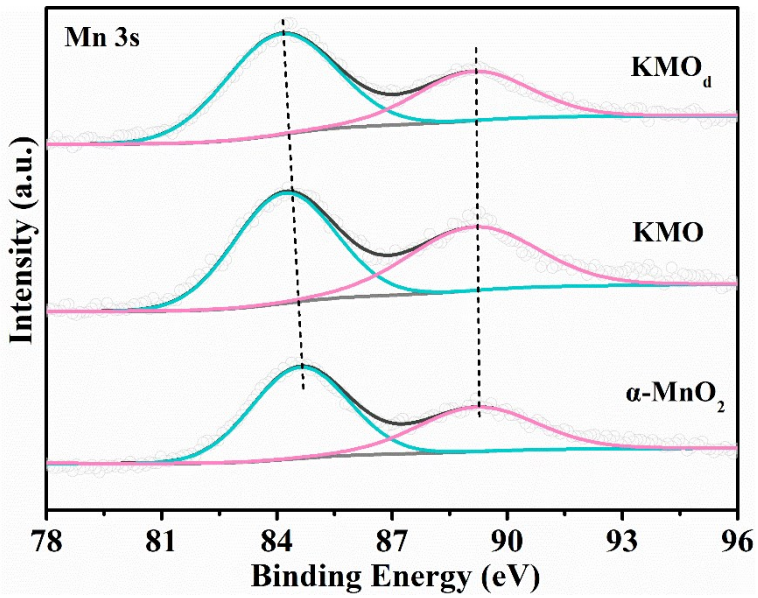

Fig. S5 Mn 3s high-resolution XPS spectra of KMO_d, KMO, and α-MnO_2. The gradual increase of Mn 3s multistate splitting distance in KMO and KMO_d indicating the gradual decrease of Mn valence from α-MnO_2 to KMO, and further from KMO to KMO_d.

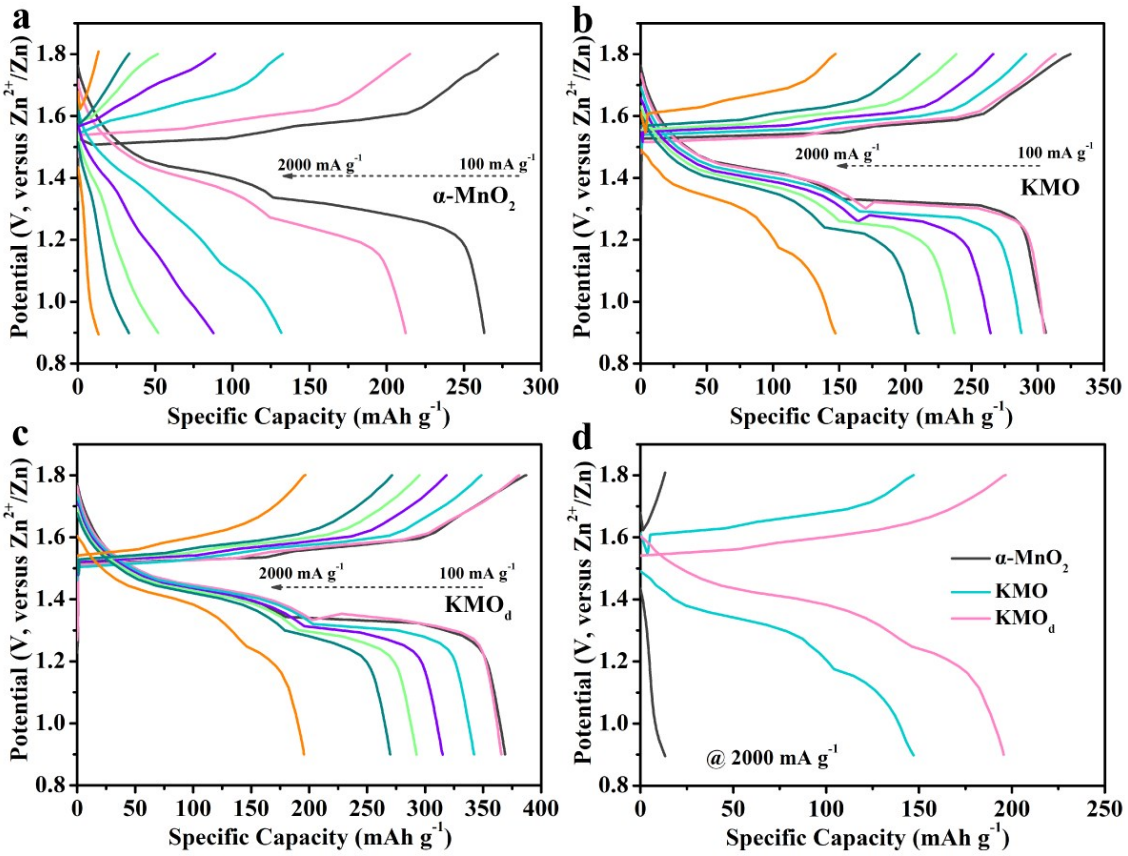

Fig. S6 Galvanostatic charge-discharge curves at different current densities of (a) α-MnO_2, (b) KMO, and (c) KMO_d electrodes. (d) Galvanostatic charge/discharge curves of KMO_d, KMO, and α-MnO_2 electrodes at 2000 mA g^{-1}.

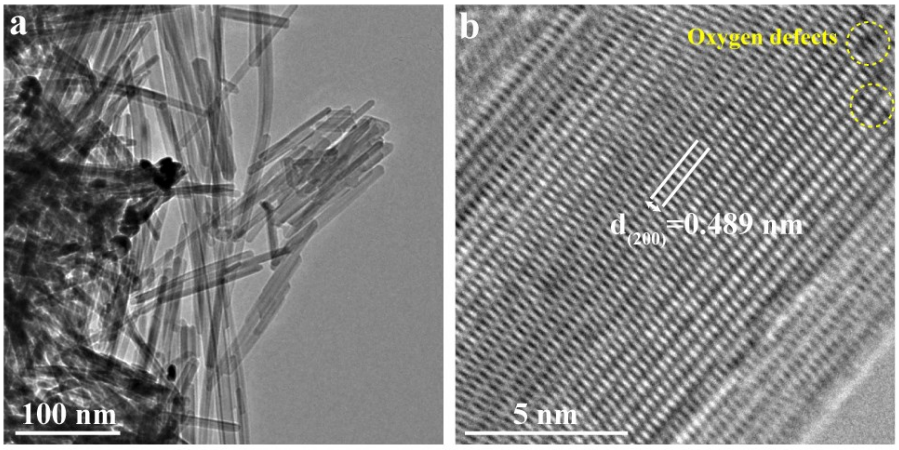

Fig. S7 (a) TEM image and (b) high-resolution TEM image of α-MnO_2-D.

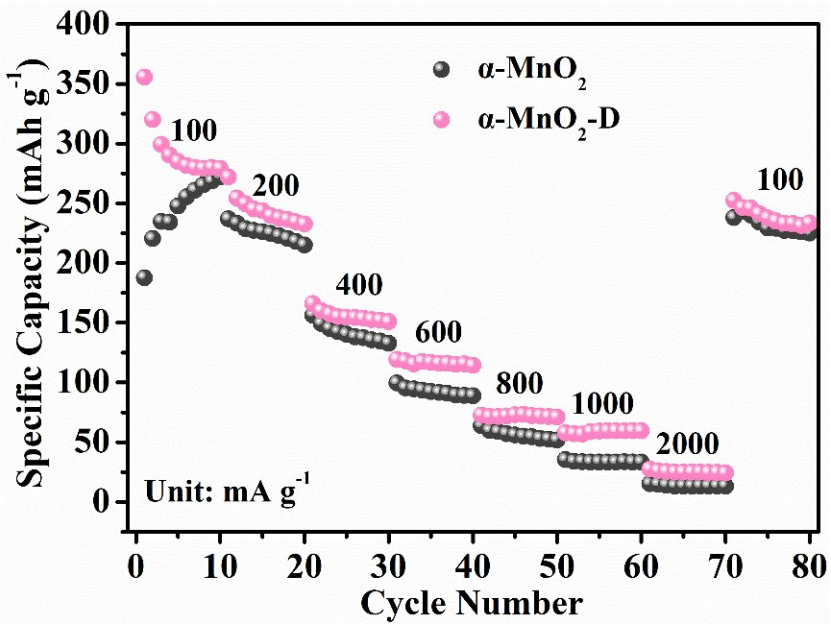

Fig. S8 Rate capability of α-MnO_2 and α-MnO_2-D cathodes.

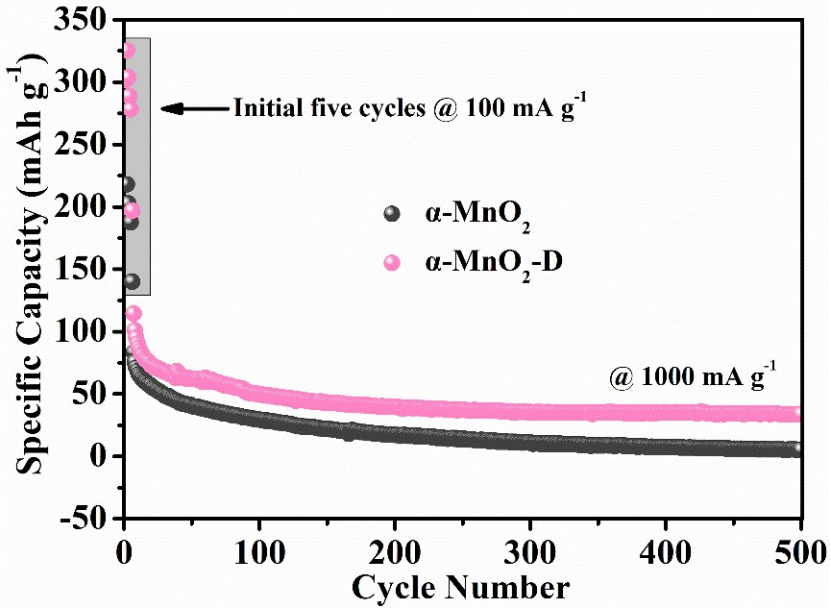

Fig. S9 Cycling performance of α-MnO_2 and α-MnO_2-D cathodes.

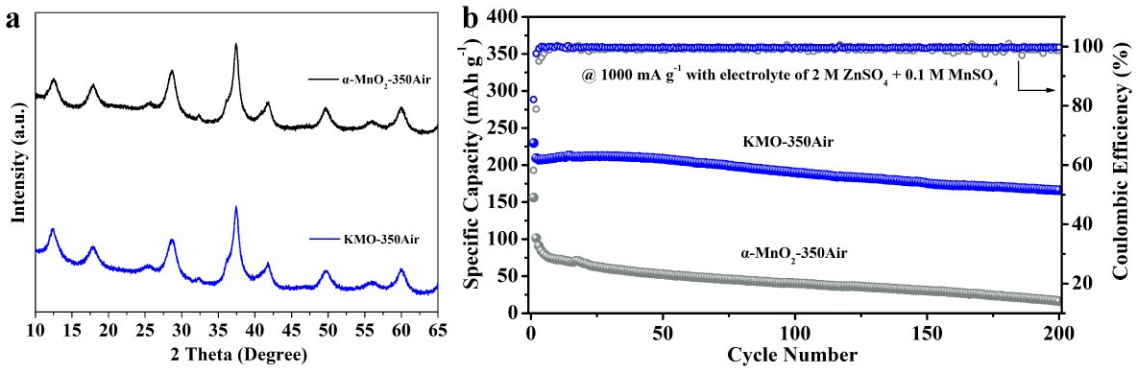

Fig. S10 (a) XRD spectra and (b) cycling performance in 2 M $ZnSO_4$ + 0.1 M $MnSO_4$ at 1000 mA g^{-1} of α-MnO_2-350Air and KMO-350Air cathodes.

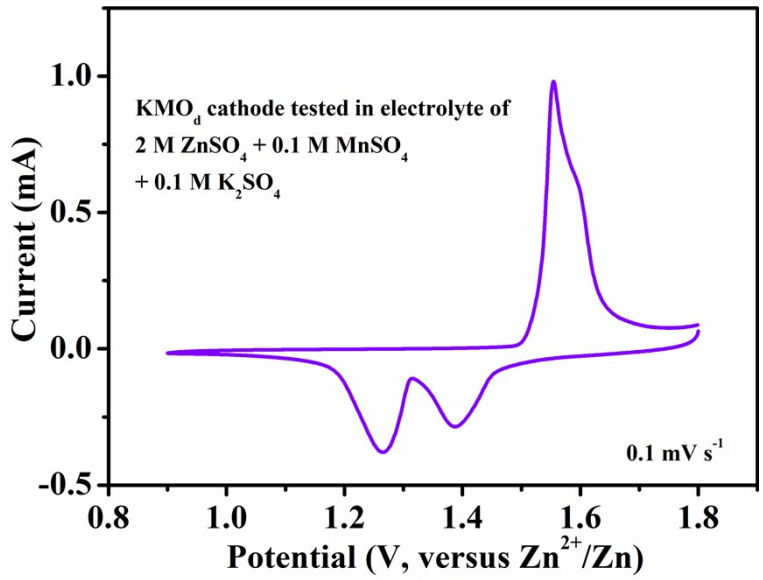

Fig. S11 CV profile of the Zn/KMO_d battery tested in electrolyte with K_2SO_4 additive at 0.1 mV s^{-1}.

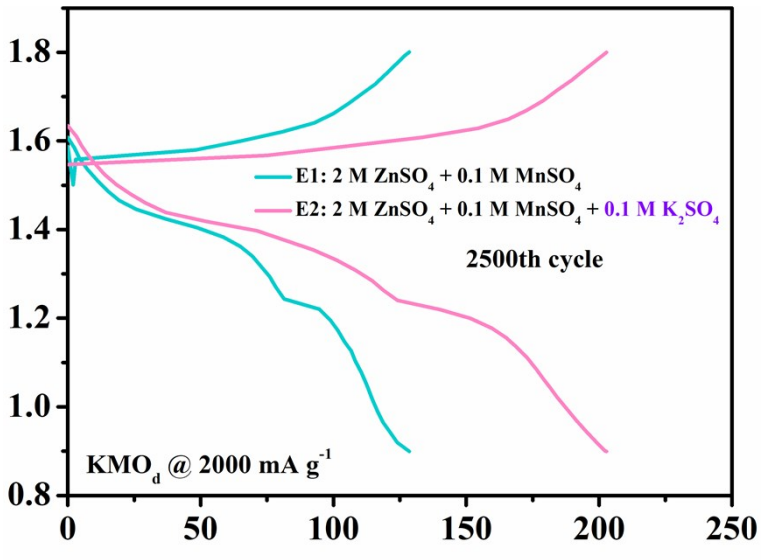

Fig. S12 Charge-discharge profiles of the 2500th cycle for KMO_d electrode at 2000 mA g^{-1} in electrolytes of 2 M $ZnSO_4$ and 0.1 M $MnSO_4$ without/with 0.1 M K_2SO_4 as an additive.

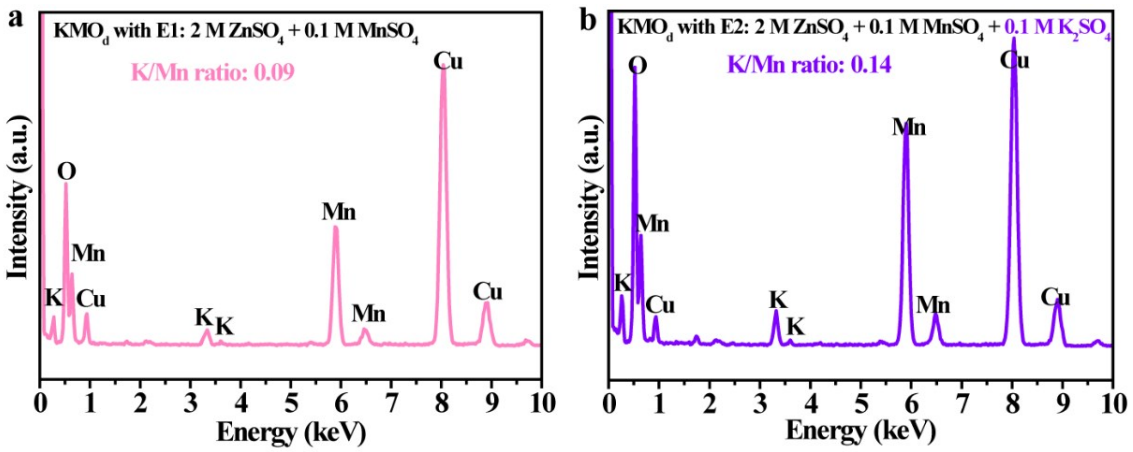

Fig. S13 Energy dispersive X-ray (EDX) spectra of KMO_d electrode after 2500 cycles at 2000 mA g^{-1} in aqueous electrolytes of (a) 2 M $ZnSO_4$ and 0.1 M $MnSO_4$ and (b) with 0.1 M K_2SO_4 as an additive.

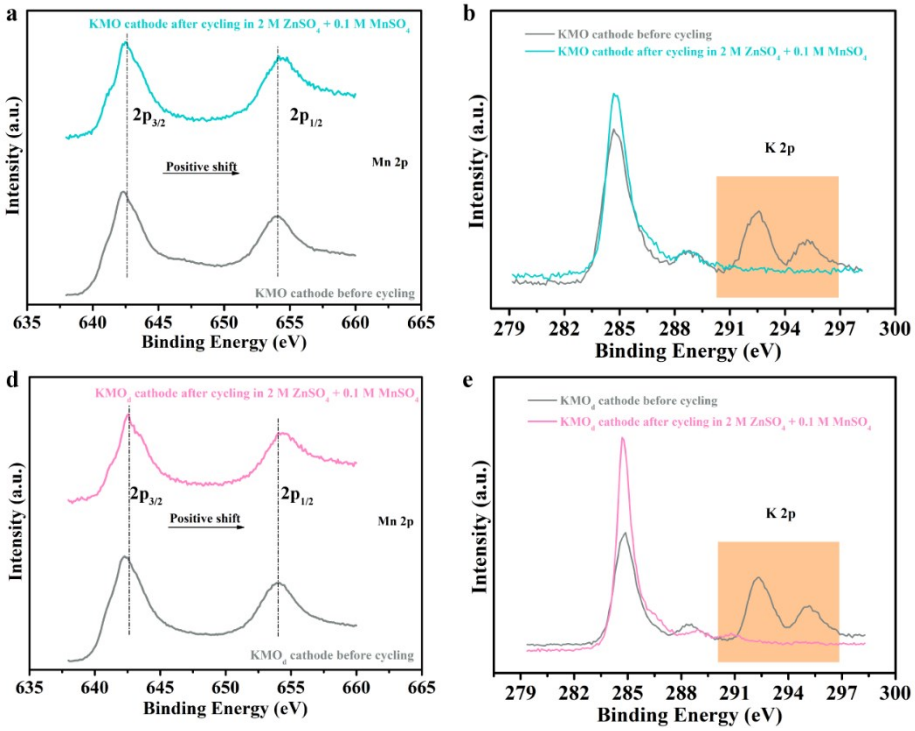

c

ICP-OES Results	
Samples	**K/Mn ratio**
KMO	**0.08**

f

ICP-OES Results	
Samples	**K/Mn ratio**
KMO_d	**0.11**

Fig. S14 Mn 2p and K 2p XPS spectra of KMO (a, b) and KMO_d (d, e) cathodes before cycling and after 300 cycles at 1000 mA g^{-1} in aqueous electrolytes of 2 M $ZnSO_4$ + 0.1 M $MnSO_4$. (c, f) ICP-OES results of KMO and KMO_d cathodes after 300 cycles at 1000 mA g^{-1} in aqueous electrolytes of 2 M $ZnSO_4$ + 0.1 M $MnSO_4$.

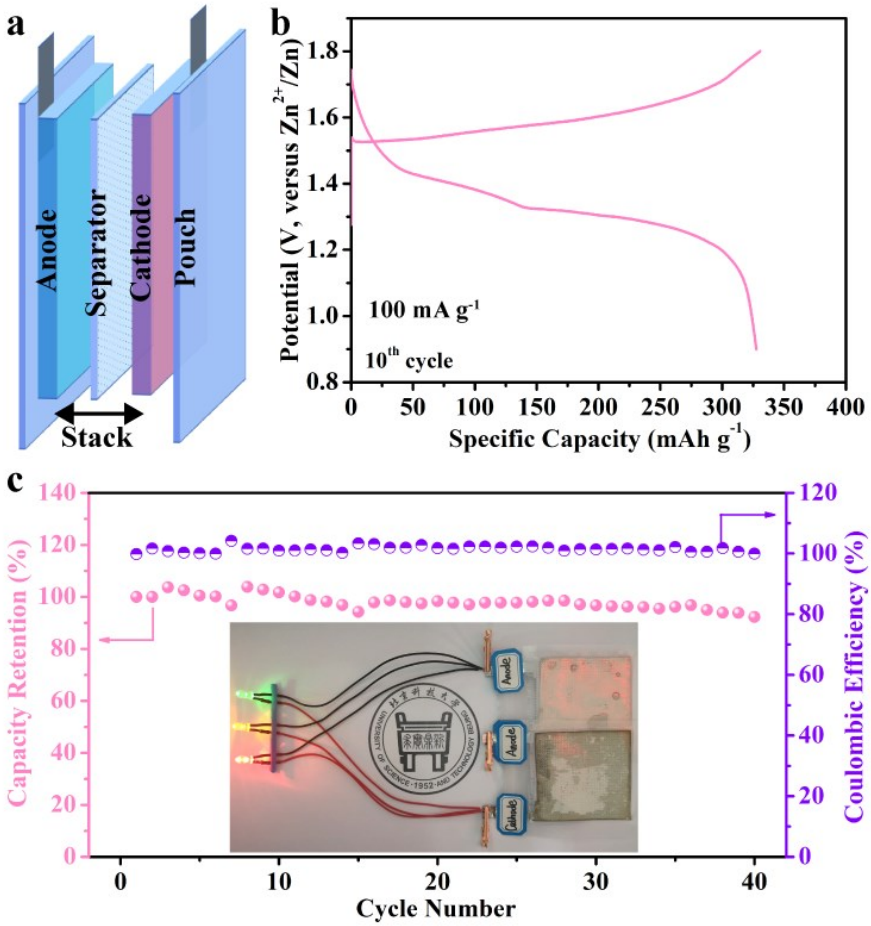

Fig. S15 (a) Illustration of the soft-packed battery configuration with anode-separator-cathode stack. (b) Charge-discharge profiles of the 10th cycle and (c) capacity retention and CE of Zn-KMO_d soft-packed battery at 100 mA g^{-1} in electrolyte of 2 M $ZnSO_4$ and 0.1 M $MnSO_4$ with 0.1 M K_2SO_4 as an additive. The inset shows that three LED lights can be lightened by two soft-packaged batteries.

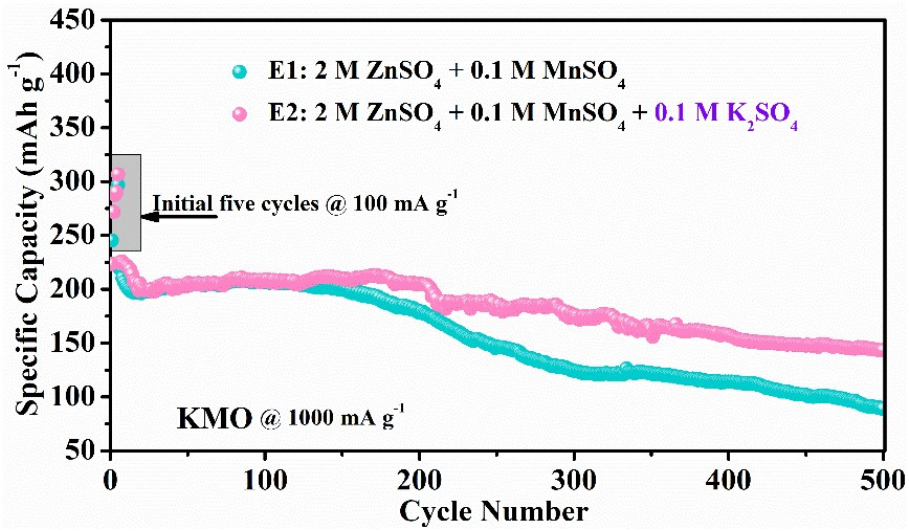

Fig. S16 Cycling performance of KMO electrode at 1000 mA g^{-1} in 2 M $ZnSO_4$ and 0.1 M $MnSO_4$ electrolytes with/without 0.1 M K_2SO_4 as an additive.

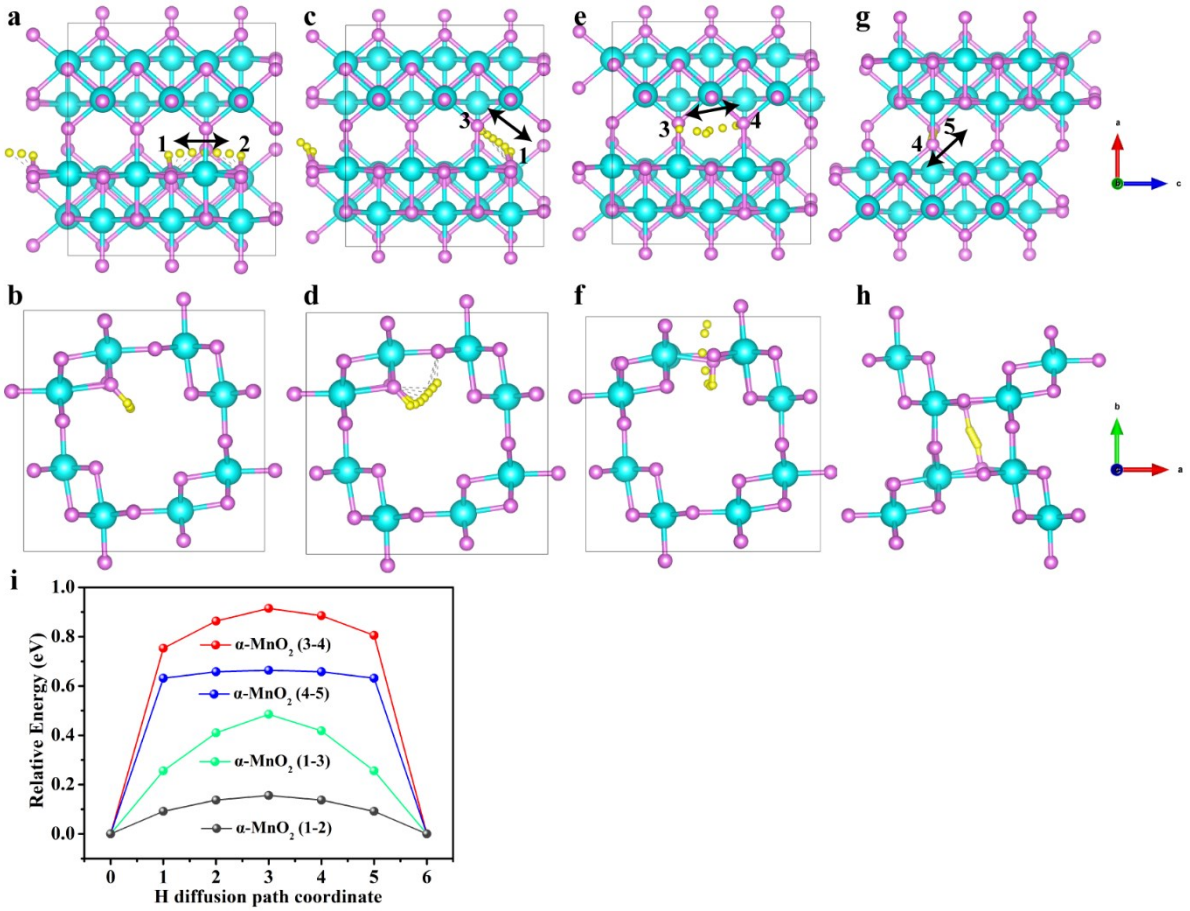

Fig. S17 (a-h) Optimized supercells and H^+ diffusion paths in α-MnO_2. The yellow spheres represent the H atom. (i) The corresponding energy variations and energy barriers for H^+ diffusion along different paths in α-MnO_2.

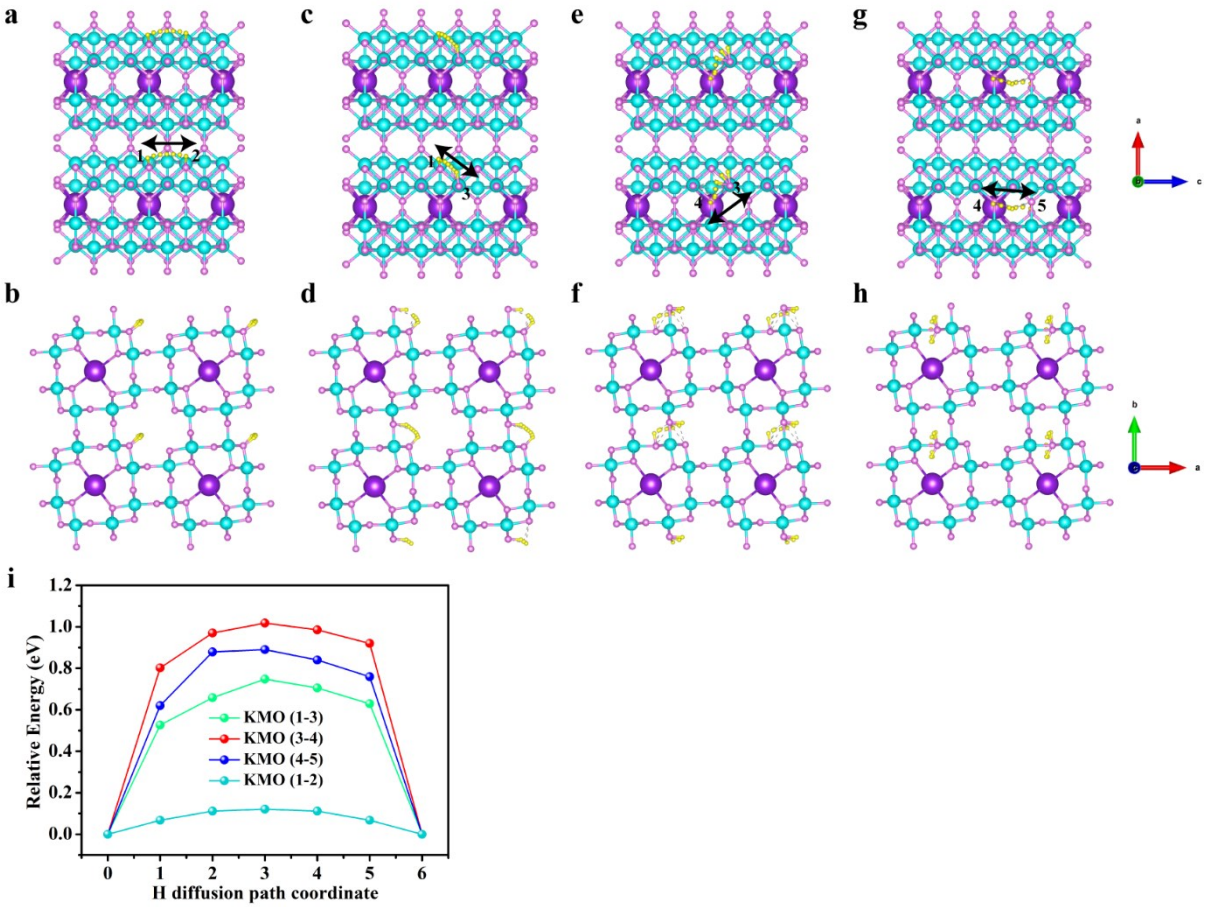

Fig. S18 (a-h) Optimized supercells and H^+ diffusion paths in KMO. The yellow spheres represent the H atom. (i) The corresponding energy variations and energy barriers for H^+ diffusion along different paths in KMO.

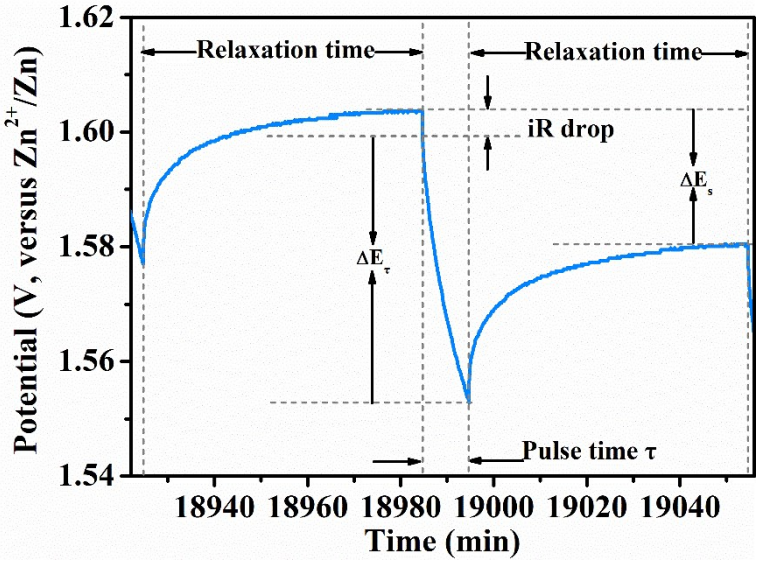

Fig. S19 E versus t curves of KMO_d electrode for a single GITT during discharge process.

The solid diffusion coefficients were measured by Galvanostatic Intermittent Titration Technique (GITT) and calculated based on the Equation (1) below:[1]

$$D_{GITT} = \frac{4}{\pi\tau}\left(\frac{m_B V_m}{M_B S}\right)^2\left(\frac{\Delta E_s}{\Delta E_\tau}\right)^2 \quad \left(\tau \ll \frac{L^2}{D_{GITT}}\right) \tag{1}$$

Where m_B (g) is the weight of the active materials, M_B (g/mol) is the molecular weight, V_m (cm^3/mol) is its molar volume, S (cm^2) is the surface area, τ (s) is duration time of the current pulse, ΔE_s is the voltage difference measured at the end of the relaxation period for two successive steps, ΔE_τ is the difference between the initial voltage and final voltage during the discharge pulse time τ after eliminating the iR drop, L is the thickness of electrode. If the voltage was linearly related to the $\tau^{1/2}$, above equation can be simplified as the following Equation (2):[2]

$$D_{GITT} = \frac{4}{\pi\tau}\left(\frac{m_B}{\rho S}\right)^2\left(\frac{\Delta E_s}{\Delta E_\tau}\right)^2 \tag{2}$$

Where ρ is the density of active materials.

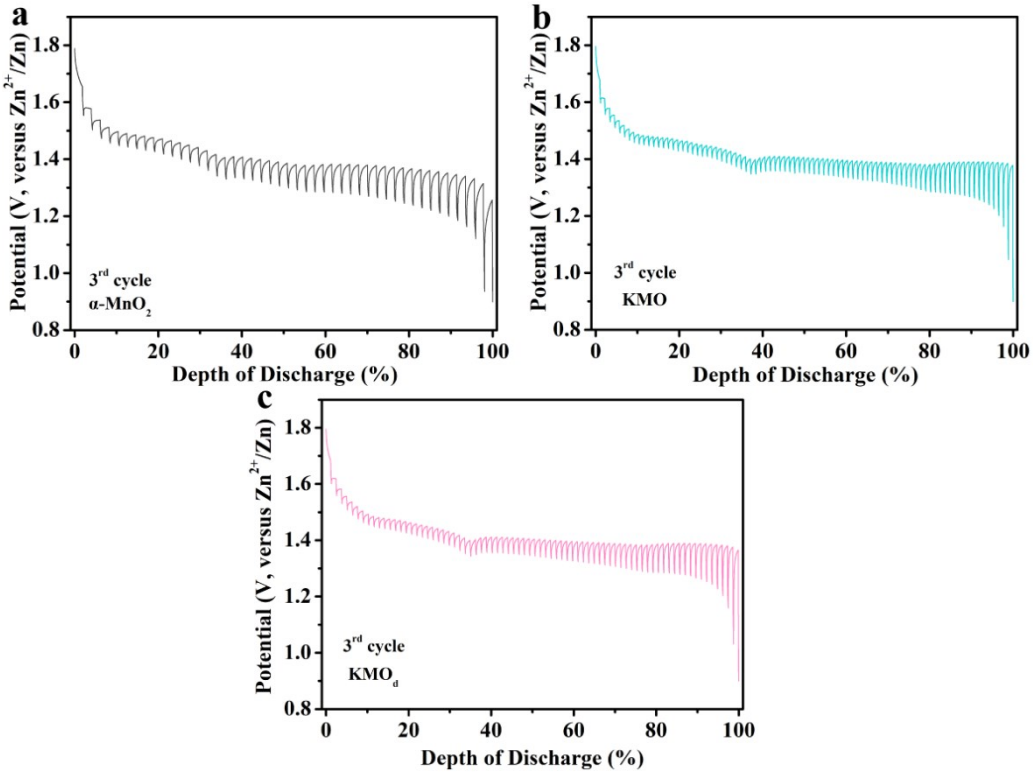

Fig. S20 The GITT curves of (a) α-MnO_2, (b) KMO, and (c) KMO_d electrodes.

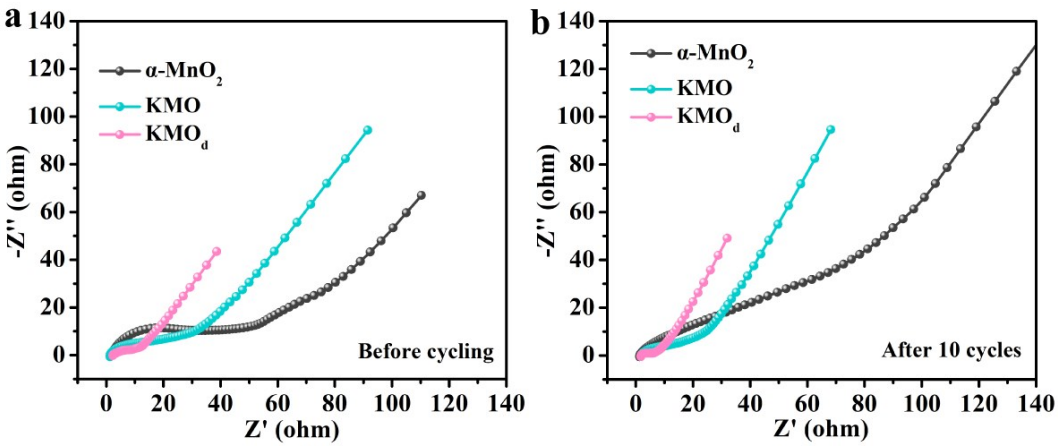

Fig. S21 Nyquist plots of KMO_d, KMO, and α-MnO_2 electrodes (a) before cycling and (b) after 10 cycles.

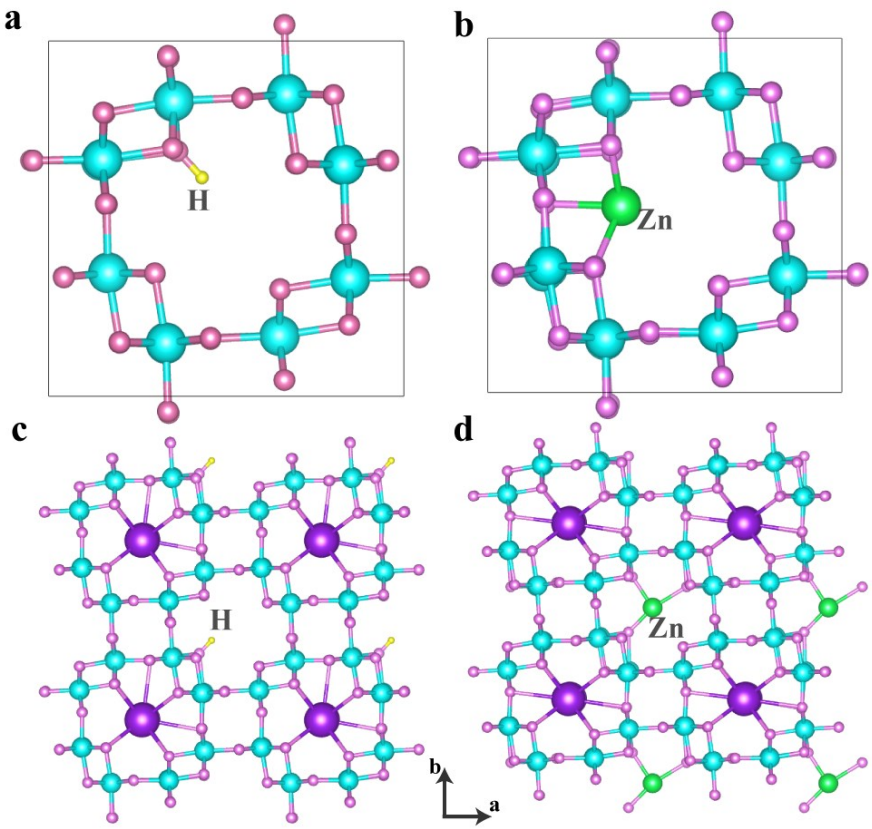

Fig. S22 The adsorption structures for H^+ and Zn^{2+} of (a,b) α-MnO_2 and (c,d) KMO.

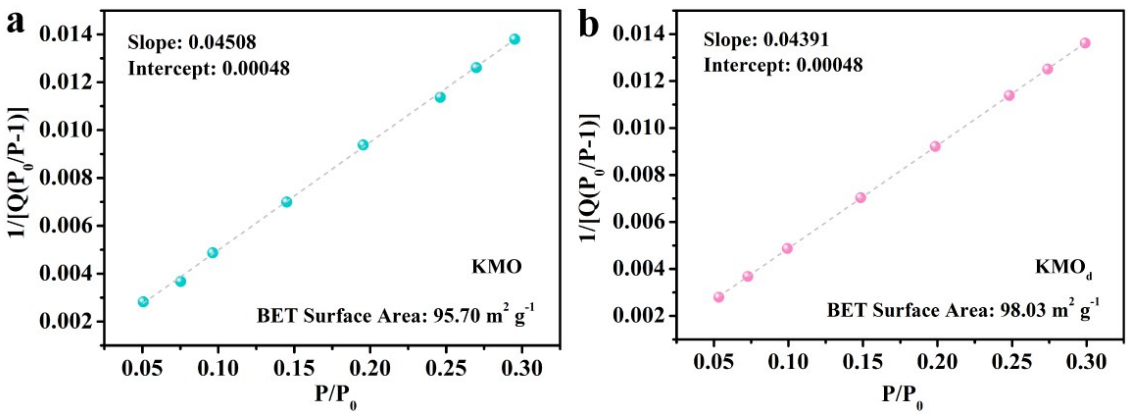

Fig. S23 The BET surface area plots of (a) KMO and (b) KMO_d.

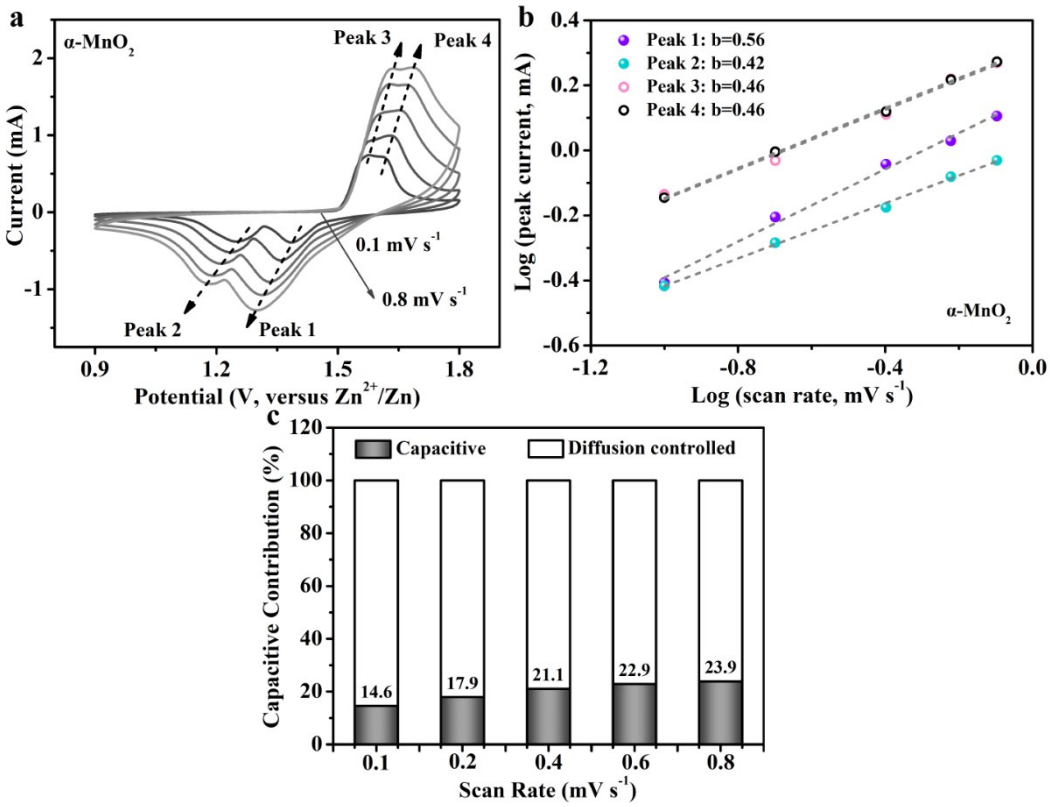

Fig. S24 (a) Cyclic voltammetry (CV) curves at different scan rates, b) the corresponding linear relationship of log(*v*) and log(*i*) at different potentials, and c) the corresponding percent of pseudocapacitive contribution of α-MnO_2 electrode.

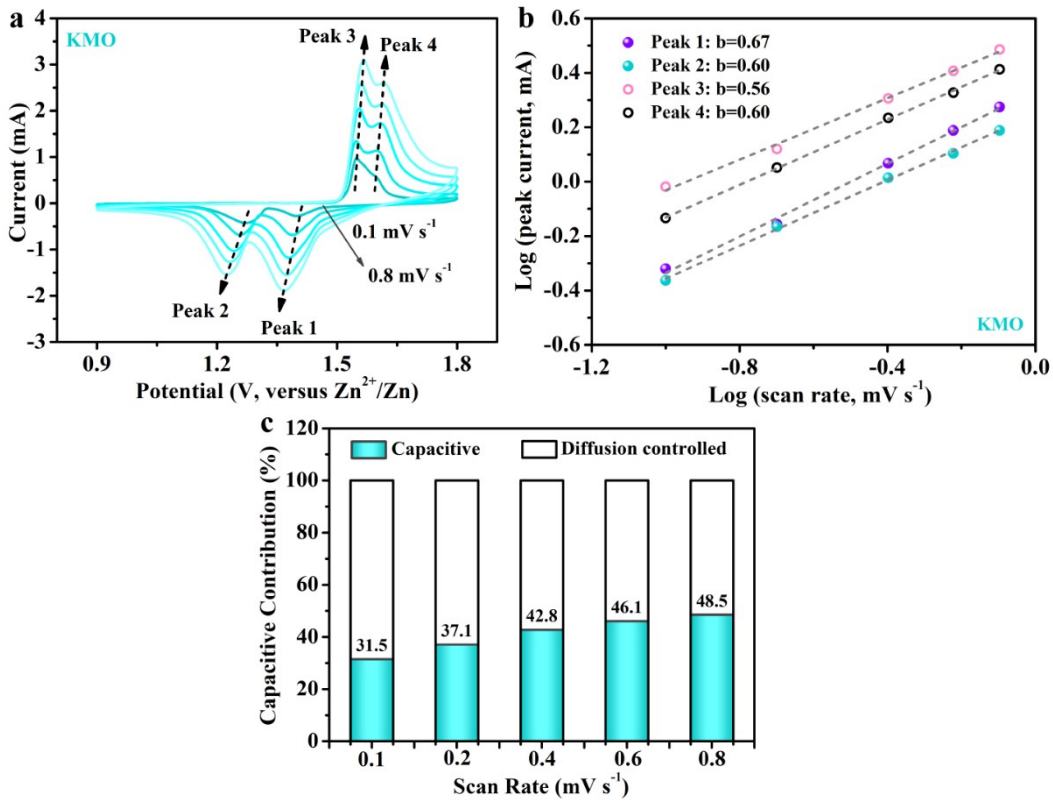

Fig. S25 (a) Cyclic voltammetry (CV) curves at different scan rates, b) the corresponding linear relationship of log(*v*) and log(*i*) at different potentials, and c) the corresponding percent of pseudocapacitive contribution of KMO electrode.

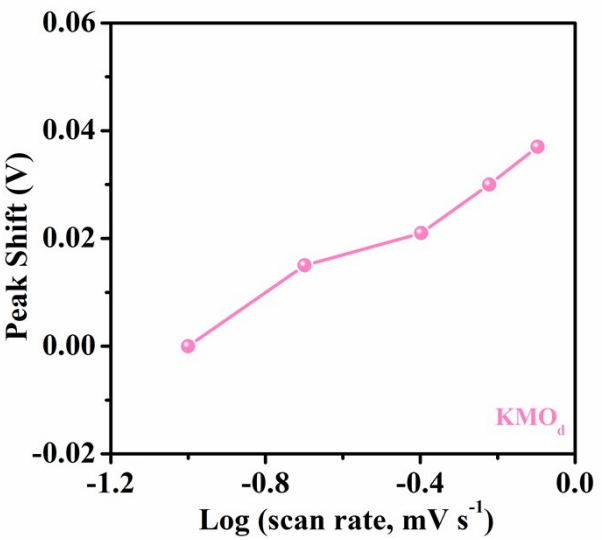

Fig. S26 Variation of the cathodic peaks voltage with different scan rates.

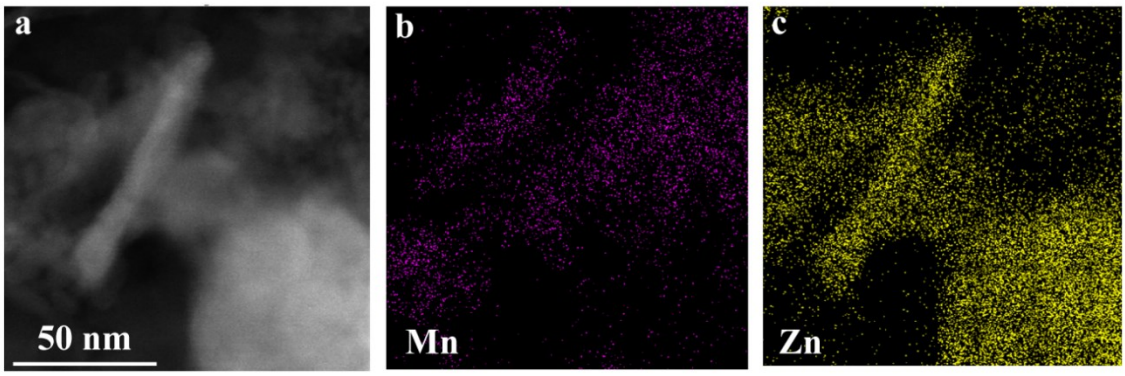

Fig. S27 (a) STEM-HAADF image, and (b,c) EDX mappings of the elemental distributions of Zn and Mn in KMO_d nanowire at fully discharged state.

Table S1. The mass loadings of different active materials shown in Fig. 3d.

Active materials	Mass loadings/ mg cm^{-1}	References
$K_{0.15}MnO_d$ (This work)	1.2	-
$K_{0.1}MnO_2$	unknown	Adv. Funct. Mater. 2019, 29, 1808375
$K_{0.19}MnO_2$	1.0	J. Mater. Chem. A, 2019, 7, 20806-20812
Ni-$K_{0.12}MO{\cdot}0.208H_2O$	1.5	Angew. Chem. Int. Ed. 2021, 60, 4169-4174
O_d-MnO_2	1.0	Adv. Energy Mater. 2019, 9, 1803815
δ-MnO_2	unknown	Electrochem. Commun. 2015, 60, 121-125
Todorokite-MnO_2	2.0	Electrochimica Acta, 2013, 112 138-143
$ZnMn_2O_4$	2.0	J. Am. Chem. Soc. 2016, 138, 12894-12901
ZnHcF	unknown	Adv. Energy Mater. 2015, 5, 1400930
CuHcF	unknown	ChemSusChem 2015, 8, 481-485

Table S2. Electrochemical performance of MnO_2-based cathodes for aqueous ZIBs.

Cathodes	Energy density (Wh kg^{-1})	Power density (W kg^{-1})	Cycle stability	Ref.
KMO_d	**518**	**1884**	**271 mAh g^{-1} at 1000 mA g^{-1} with 97.5% capacity retention after 500 cycles; 203 mAh g^{-1} at 2000 mA g^{-1} with 81.3% capacity retention after 2500 cycles**	**This work**
MnO_2	231	4000 (9C)	100 mAh g^{-1} at 344 mA g^{-1} with 55.6% capacity retention after 150 cycles	[3]
O_d-MnO_2	470	10^4 (30 A g^{-1})	105 mAh g^{-1} at 5000 mA g^{-1} with 84% capacity retention after 2000 cycles	[4]
β-MnO_2	385	-	134 mAh g^{-1} at 1250 mA g^{-1} with 83.2% capacity retention after 1000 cycles	[5]
$K_{0.19}MnO_2$	380	403	180 mAh g^{-1} at 1540 mA g^{-1} with 90% capacity retention after 400 cycles	[6]
KMO	398	2750	156 mAh g^{-1} at 1000 mA g^{-1} after 1000 cycles	[7]
β-MnO_2	-	-	135 mAh g^{-1} at 200 mA g^{-1} with 75% capacity retention after 200 cycles	[8]
MnO_x@N-C	390	1900	100 mAh g^{-1} at 2000 mA g^{-1} after 1600 cycles	[9]
Ni-doped KMO	421	1766	120 mAh g^{-1} at 1232 mA g^{-1} with 71.4% capacity retention after 2000 cycles	[10]
α-MnO_2@G	407	9450	240 mAh g^{-1} at 1000 mA g^{-1} after 100 cycles	[11]
D-MnO_2	406	4100	250 mAh g^{-1} at 1000 mA g^{-1} after 500 cycles	[12]

Table S3. The optimized lattice constants of KMO_d, KMO, and α-MnO_2 unit cells.

	α-MnO_2	KMO	KMO_d
a/Å	9.687819	9.71956	9.775119
b/Å	9.687819	9.71956	9.711212
c/Å	2.890018	5.808683	5.816079
α/°	90	90	90
β/°	90	90	90
γ/°	90	90	90

References

[1] D. T. Ngo, H. T. T. Le, C. Kim, J.-Y. Lee, J. G. Fisher, I.-D. Kim, C.-J. Park, *Energy Environ. Sci.* 2015, **8**, 3577.

[2] X. H. Rui, N. Ding, J. Liu, C. Li and C. H. Chen, *Electrochimica Acta* 2010, **55**, 2384.

[3] Y. Li, S. Wang, J. R. Salvador, J. Wu, B. Liu, W. Yang, J. Yang, W. Zhang, J. Liu, J. Yang, *Chem. Mater.* 2019, **31**, 2036.

[4] T. Xiong, Z. G. Yu, H. Wu, Y. Du, Q. Xie, J. Chen, Y. W. Zhang, S. J. Pennycook, W. S. V. Lee, J. Xue, *Adv. Energy Mater.* 2019, **9**, 1803815.

[5] M. Liu, Q. Zhao, H. Liu, J. Yang, X. Chen, L. Yang, Y. Cui, W. Huang, W. Zhao, A. Song, Y. Wang, S. Ding, Y. Song, G. Qian, H. Chen, F. Pan, *Nano Energy* 2019, **64**, 103942.

[6] G. Liu, H. Huang, R. Bi, X. Xiao, T. Ma, L. Zhang, *J. Mater. Chem. A* 2019, *7*, 20806.

[7] G. Fang, C. Zhu, M. Chen, J. Zhou, B. Tang, X. Cao, X. Zheng, A. Pan, S. Liang, *Adv. Funct. Mater.* 2019, **29**, 1808375.

[8] S. Islam, M. H. Alfaruqi, V. Mathew, J. Song, S. Kim, S. Kim, J. Jo, J. P. Baboo, D. T. Pham, D. Y. Putro, Y. Sun, J. Kim, *J. Mater. Chem. A* 2017, **5**, 23299.

[9] Y. Fu, Q. Wei, G. Zhang, X. Wang, J. Zhang, Y. Hu, D. Wang, L. Zuin, T. Zhou, Y. Wu, S. Sun, *Adv. Energy Mater.* 2018, **8**, 1801445.

[10] Q. Zhao, A. Song, W. Zhao, R. Qin, S. Ding, X. Chen, Y. Song, L. Yang, H. Lin, S. Li, F. Pan, *Angew. Chem. Int. Ed.* 2021, https://doi.org/10.1002/anie.202011588.

[11] B. Wu, G. Zhang, M. Yan, T. Xiong, P. He, L. He, X. Xu, L. Mai, *Small* 2018, **14**, 1703850.

[12] J. Wang, J. Wang, X. Qin, Y. Wang, Z. You, H. Liu, M. Shao, *ACS Appl. Mater. Inter.* 2020, **12**, 34949.